44th AIAA Aerospace Sciences Meeting and Exhibit
9 - 12 January 2006, Reno, Nevada

AIAA 2006-1192

Simulation and Analysis of Rarefied Parallel Interacting Sonic Jets

Wenhai Li* and Foluso Ladeinde†
Mechanical Engineering Department, SUNY at Stony Brook, Stony Brook, NY 11794-2300

The interaction effects between two rarefied parallel sonic jets are studied. When the flow is in the free or near-free molecular regime, in which case the interaction effects are weak, the density profile of the flow field can be approximated by the summation of the density profiles of the individual jets using an asymptotic model developed by Ashkenas and Sherman.[1] This explains the existence of the self-similarity of the flow field for the density profile, which was discovered by Zhu and Dagum.[2-4] For the flow in the continuum or near-continuum regime, in which case the interaction effects are strong, self-similarity does not hold and interaction shock waves are formed. To analyze the influence of the interaction shock wave, a modified Penetration Knudsen Number has been introduced. It is shown that the existence of the interaction shock wave significantly decreases molecular penetration. This effect is shown in the density profiles from the DSMC calculation. The translational non-equilibrium in the interaction region is also analyzed from the DSMC results.

Nomenclature

c_r	=	relative velocity of molecular pairs
c'	=	molecular thermal velocity
D	=	diameter of jet orifice
d	=	diameter of gas molecule
L	=	separation distance between the orifices of two jets
l_{ref}	=	reference length
Kn	=	Knudsen number
Kn_p	=	penetration Knudsen number
n	=	number density
r	=	polar distance
T	=	temperature
t	=	time
u_{max}	=	maximum velocity
Z_r	=	rotational collision number
γ	=	specific heat ratio
δ	=	height of shock wave front
θ	=	polar angle
λ	=	molecular mean free path
ρ	=	density
σ_T	=	total collision cross-section
τ_c	=	molecular mean collision time
φ	=	angle between shock front and x-axis
χ	=	density ration in front of and behind of shock front

Subscripts

0	=	properties at orifice exit

* Graduate Research Assistant.
† Associate Professor, Life Member and Associate Fellow of AIAA.

s = properties under stagnation condition
t = overall flow field properties

Superscripts

$*$ = properties with the influence of shock waves.

I. Introduction

WITH the rapid development of space technology, a lot of emphasis has been placed on the study of the interaction between rarefied free jets. Various jet interaction phenomena exist in the design of spacecraft, one example being multi-nozzle rockets (Fig. 1). The rockets are always equipped with two or more nozzles to provide large impulse and stability. Because of the high altitude, the pressure is low, which causes the plumes from each nozzle to have a large radial extent. Therefore, an interaction between the neighboring plumes may occur. Another example is the spacecraft's Orbiter Reaction Control System (RCS), which always comprises of many primary and vernier engines. The RCS can provide the thrust for altitude maneuvers and small velocity changes along the orbiter axis by firing the selected engines. If adjacent engines are fired simultaneously, an interaction between the two jets can occur. The jet interaction phenomena can also be seen in a satellite's Altitude Control System (ACS), which is used to control the altitude of the satellite. This system is generally formed by an array of small thrusters. Because the size of the satellite is small and the plume size is large in high altitude, jet interaction between the adjacent plumes can be observed.

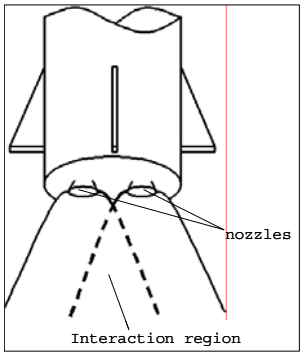

Figure 1. Jet interaction in multi-nozzle rocket

The interaction between the jets can greatly change the flow profile, the mixing pattern of the products of combustions, and the dynamics of jet impingement. These phenomena can cause a lot of difficulties in the design of a spacecraft. Therefore, jet interaction is important and needs to be investigated in detail. When the interactions take place in the continuum regime, the problem can be solved using the classical continuum method, such as the solution of the Navier-Stokes equations. However, when the interactions take place at a high altitude, where rarefaction effects become significant, the continuum method will not be applicable. The problem needs to be attacked from the standpoint of rarefied gas dynamics (RGD).

Only a few studies have been carried out on rarefied interacting jets. Koppenwallner and Dankert[5-6] first studied the scaling laws for rarefied jet interaction and suggested a parameter, which is called the Penetration Knudsen number, Kn_p, to characterize the plume-plume penetration effects. Soga[7] and Niimi[8] observed the flow field of the interacting jets in experiments using the electron beam and planar laser-induced fluorescence, respectively. Zhu and Dagum[2-4] first simulated the rarefied jet interaction with the Direct Simulation Monte Carlo (DSMC) method.

II. Flow in the free or near-free molecular regime

The study of plume-plume interaction is based on the theory of a single rarefied plume, which can usually be predicted by an analytical formula. The use of asymptotic models to predict the rarefied jet flow field is common. These models are based on the assumption[5] that in the far field of the plume, the flow velocity has reached its adiabatic speed limit $u_{\max}$, and that all streamlines are radial and straight, as if they emanate from the same source

point in the orifice exit (Fig. 2). Based on the continuity of mass, the flow density attenuates along the streamline by $1/r^2$ and it is given by

$$\frac{\rho}{\rho_s} = \frac{n}{n_s} = A\left(\frac{D}{r/2}\right)^2 \cdot f(\theta), \tag{1}$$

where ρ_s and n_s are stagnation density and number density, r and θ are polar distance and angle to the orifice exit and D is orifice diameter. A is a constant determined by the gas species and $f(\theta)$ is a plume angular density decay function, which is given by

$$f(\theta) = \cos^k\left(\frac{\pi}{2}\cdot\frac{\theta}{\theta_{\max}}\right), \tag{2}$$

where $\theta_{\max}$ is an angular scale. k is a constant that depends on gas specific heat ratio γ. Different researchers have used different values for k. Ashkenas and Sherman[1] used $k = 2$, Albini[9] and Hubbard[10] used k=1/(γ-1), while Boyton[11] suggested k=2/(γ-1).

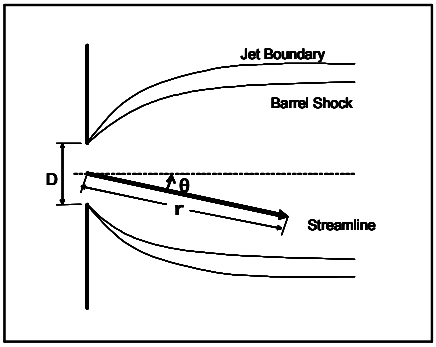

Figure 2. Asymptotic model for one rarefied free jet

When the jets' stagnation Knudsen Number Kn_s is very small or the separation distance (L/D) between the two jets' orifices is very large, the flow is in the free molecular regime and the interaction between the two jets can be neglected. In these cases, the overall number density profile of the flow field can be evaluated as the sum of the number density of all the plumes, such that

$$n_{total} = n_{jet,1} + n_{jet,2}, \tag{3}$$

where n_{total}, $n_{jet,1}$ and $n_{jet,2}$ are, respectively, the total number density, number density of jet 1, and number density of jet 2 (shown in Fig. 3). Substituting Eqn. (1) into Eqn. (3), we can obtain the expression for the density profile along the symmetry axis $(x,0,0)$ as

$$\frac{\rho_t(x/D)}{\rho_s} = 2A\cdot\left(\frac{D}{r/2}\right)^2 \cdot f(\theta) = 2A\cdot\left(\frac{D}{L}\right)^2 \cdot \sin^2\theta\cdot\cos^k\left(\frac{\pi}{2}\cdot\frac{\theta}{\theta_{\max}}\right) = 2A\cdot\left(\frac{D}{L}\right)^2 \cdot g(\theta), \tag{4}$$

where

$$\theta = \arctan\left(\frac{1}{2}\frac{L/D}{x/D}\right) \tag{5}$$

and

$$g(\theta) = \cos^k\left(\frac{\pi}{2}\cdot\frac{\theta}{\theta_{\max}}\right)\cdot\sin^2\theta\,. \tag{6}$$

Zhu[3,4] observed a self-similar phenomenon based on $(L/D)^2$ in the interaction region. This can be illustrated from Eqn. (4) with the fact that $\left(\rho_t/\rho_s\right) \propto (L/D)^{-2}$.

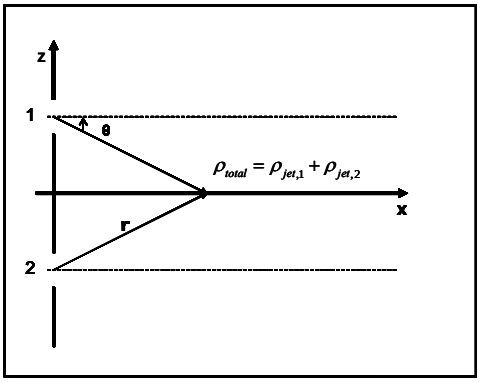

Figure 3. Interacting jets for $Kn_s \to \infty$

III. Flow in the continuum or near-continuum regime

When the flow is in the continuum or near-continuum regime, the interaction effects are strong and the above asymptotic model is not directly applicable. For this purpose, several previous studies have been carried out to characterize plume-plume interaction. Koppenwallner[5] derived the scaling laws for rarefied jet interaction and introduced a parameter to evaluate the molecular penetration between the two plumes. The parameter is called the Penetration Knudsen Number, Kn_p. Here, we briefly recall the definition of Kn_p following the 1984 paper of Koppenwallner. Kn_p is defined as follows:

$$Kn_p = \frac{\lambda_p}{l_{ref}}, \tag{7}$$

where λ_p is the mean distance of plume 1 molecules moving through plume 2 flow field and l_{ref} is selected as the distance from the symmetry plane to the centerline of plume 2 (shown in Fig. 4).

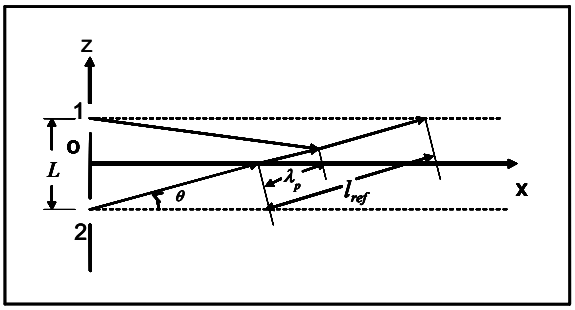

Figure 4. Definition of the Penetration Knudsen Number in rarefied jet interaction

The expressions for l_{ref} and λ_p are given as[5]

$$l_{ref} = \frac{L/2}{\sin\theta} \tag{8}$$

and[12]

$$\lambda_p = \lambda_{12} = \left(n_2 \cdot \sigma_{T,12} \cdot \frac{c_{r,12}}{c_1'} \right)^{-1}, \tag{9}$$

respectively, where $\sigma_{T,12} = \pi d^2$ is the total collision cross-section between the two plume molecules, d is molecular diameter, and $c_{r,12}$ is the relative velocity between the molecules from the two jets, which is calculated as[5]

$$c_{r,12} = 2\sin\theta \cdot u_{\max}. \tag{10}$$

The mean thermal velocity, c'_1, of the jet molecules can be defined as[12]

$$c_1' = \frac{2}{\sqrt{\pi}}\sqrt{2RT_0}, \tag{11}$$

where T_0 is the temperature at the orifice exit. For sonic free jets, $u_{\max}$ is the adiabatic speed limit given by[13]

$$u_{\max} = \sqrt{\frac{2\gamma}{\gamma+1}RT_0}. \tag{12}$$

Eqn. (9) can now be expressed in the form

$$\lambda_p = \frac{1}{\pi d^2 \cdot n_i} \frac{\sqrt{1+1/\gamma}}{\sin\theta\sqrt{\pi}}, \tag{13}$$

where n_i is the number density of one primary jet, which can be evaluated from Eqn. (1). Substituting Eqns. (8) and (13) into Eqn. (7) and simplifying, the Penetration Knudsen Number, Kn_p, can be obtained as

$$Kn_p(\theta) = \frac{2\sqrt{2}}{\sqrt{\pi}}\sqrt{1+\frac{1}{\gamma}} \cdot \frac{Kn_s}{A} \cdot \frac{L}{D} \cdot \frac{1}{f(\theta)\sin^2\theta} = \frac{Kn_s}{B} \cdot \frac{L}{D} \cdot \frac{1}{f(\theta)\sin^2\theta}, \tag{14}$$

where $Kn_s = \lambda_s / D = \left(\sqrt{2}\pi d^2 n_s\right)^{-1} / D$ is the Knudsen number at stagnation conditions based on the orifice diameter D, and B is a constant including all constant terms related to γ. Kn_p is a function of θ and can be converted to the following form:

$$\frac{Kn_p(\theta)}{\frac{Kn_s}{B}\cdot\frac{L}{D}} = \frac{1}{\sin^2\theta\cdot\cos^k\left(\frac{\pi}{2}\cdot\frac{\theta}{\theta_{\max}}\right)} = \frac{1}{g(\theta)}. \tag{15}$$

Eqn. (15) shows that Kn_p is also a function of $g(\theta)$, which is defined in Eqn. (6). This implies that Kn_p is a parameter that characterizes the momentum penetration between the two jets.

Although the concept of Penetration Knudsen Number defined by Koppenwallner can be used to characterize the molecular penetration, this definition cannot be used in the continuum or near-continuum regime because it is based on the assumption that there is no interaction shock wave in the flow field. This assumption is inaccurate due to the fact that the interaction shock waves are formed[8] and play a critical role in molecular penetration when interaction effects are strong. The effects of the interaction shock wave are depicted in Fig. 5. Before encountering the shock

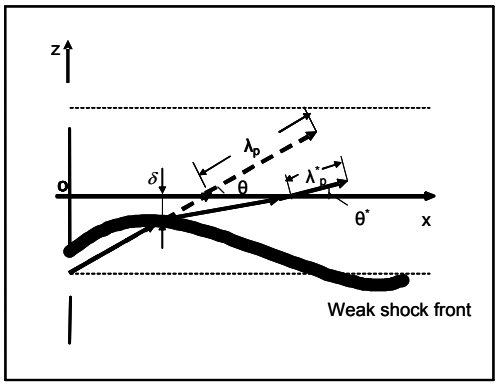

Figure 5. The influence of a shock wave

wave, the streamlines are in the radial direction and the density decays as $1/r^2$ along with the streamline. After going through the shock wave, both the stream direction and the flow density are changed. To evaluate this change, one needs to know the geometry and the strength of the shock front. Based on the assumption that the geometry of the shock front is not affected by the strength of the shock, Gidalevich[14] introduced an expression for the geometry of the shock front $\delta(x)$, which is given by

$$\frac{d\delta}{dx} = \frac{x(1-\chi_{\min}) - \left(x^2(1-\chi_{\min})^2 - \chi_{\min}(L-2\delta)^2\right)^{1/2}}{L-2\delta}, \tag{16}$$

where $\chi(x) = n(x)/n^*(x)$ is the density ratio across the shock front, and n and n^* are the density in front of and behind the shock front, respectively. When the shock wave is very strong, which means that the Mach number before the shock front goes to infinity, χ has the minimum value $\chi_{\min} = (\gamma-1)/(\gamma+1)$. ($\chi$ is a value between $\chi_{\min}$ and 1.) When the shock front is stronger, χ becomes smaller, and vice versa. The direction of the streamline is also changed from θ to θ^*. Using Rankine-Hugoniot relation, the direction of the streamline behind the shock front is given by

$$\theta^* = \arctan\left(\frac{\tan(\theta+\phi)-\frac{1}{\chi}\tan\phi}{\tan\phi\tan(\theta+\phi)+\frac{1}{\chi}}\right), \tag{17}$$

where $\phi = \arctan(d\delta/dx)$ is the angle between the tangent to the shock front and the *x*-axis. θ^* is a value between 0 and θ. When the shock is very strong, the direction of the streamline after the shock front is changed to the direction parallel to the x-axis, which means that $\theta^* = 0$.

From Eqn. (1) and the fact that the radius is $(L/2-\delta)/\sin\theta$, we can obtain the number density before the shock front as

$$n = n_s A \frac{D^2 \sin^2\theta}{4(L/2-\delta)^2}\cdot f. \tag{18}$$

Note that the mean free path $\lambda_p{}^*$ can be expressed in the form[12]

$$\lambda_p{}^* = \left(n^* \cdot \sigma_{T,12} \cdot \frac{c_r^*}{c_1'^*}\right)^{-1}. \tag{19}$$

The superscript '*' implies the existence of an oblique shock wave. To simplify the problem, we assume that the number density behind the shock front remains constant and c' is also unchanged. We can obtain the equation for the number density behind the shock front as

$$n^* = \frac{n}{\chi} = \frac{1}{\chi}\cdot n_s A \frac{D^2 \sin^2\theta}{4(L/2-\delta)^2}\cdot f. \tag{20}$$

We can also compute the relative velocity between the molecules from the two jets:

$$c_r^* = 2u_{\max}\sin\theta^* = 2u_{\max}\left(\cos(\theta+\phi)\sin\phi - \chi\sin(\theta+\phi)\cos\phi\right). \tag{21}$$

Substituting Eqns. (20) and (21) into Eqn. (19), we can write the expression for λ_p^* as

$$\lambda_p^* = \frac{2(L/2-\delta)^2\cdot\chi}{D^2 n_s A\cdot\pi d^2\sin\theta^*\cdot f}. \tag{22}$$

The mean free path with and without the shock wave are related as

$$\lambda_p^* = \lambda_p\cdot\chi(x)\cdot\left(1-\frac{\delta(x)}{L/2}\right)^2\cdot\frac{\sin\theta}{\sin\theta^*}, \tag{23}$$

where λ_p is determined from Eqn. (9). Recall the definition of the Penetration Knudsen Number in Eqn. (7) and choose the reference length as

$$l_{ref}^* = \frac{L/2}{\sin\theta^*}. \tag{24}$$

Therefore, a modified Penetration Knudsen Number can be defined as

$$Kn_p^*(\theta) = \frac{\lambda_p^*}{l_{ref}^*} = Kn_p(\theta)\cdot\chi(\theta)\cdot\left(1-\frac{\delta(\theta)}{L/2}\right)^2, \tag{25}$$

where the "unmodified" Kn_p is defined in Eqn. (14). When an interaction shock wave exists, $\chi < 1$ and $\delta < L/2$, so that $Kn_p^* < Kn_p$, which means that the shock wave reduces the molecular penetration.

IV. Numerical Method

A three-dimensional DSMC code has been developed for the simulation of the rarefied gas flows. The DSMC method has been recognized as a powerful technique capable of predicting rarefied gas flow in the regimes where neither the Navier-Stokes nor the free-molecular approaches are appropriate. In this study, the DSMC algorithm is built around the same physical concepts as described by Bird.[12]

Fig. 6 shows the three-dimensional computational domain for the simulation. The stagnation Knudsen number Kn_s used are 0.0003, 0.003, 0.03, 0.3, 3 and 10. Three separation distances $L/D = 1.5$, 3, 6 are investigated for each Kn_s. The cell dimensions need to be smaller than the local mean free path λ_L for accurate results. However, both Hass[15] and Usami[16] have shown that a coarser network is still acceptable for the general study of the flow field structure. Because the local mean free path λ_L increases rapidly along the flow streamline, finer grids are only required in a small region near the orifice exit. The domain must be large enough so that the influence of interacting jets does not reach the downstream boundary. For the cases of $L/D = 1.5$, 3 and 6, the domain geometry is set to *15D×7D×5D*, *15D×6D×6D* and *15D×4D×8D*, respectively. The domain size is determined by the following criterion: when *L/D* is small, the interaction effects are strong and more molecules are squeezed, which results in a rapid expansion rate in the *y*-direction. In this case, the computational domain needs to be enlarged in the *y*-direction. The maximum number of cells used in this study is approximately 2×10^6 for the case of small stagnation Knudsen Number ($Kn_s = 0.0003$). The sub-cell method,[12] whereby each cell is subdivided into a 2×2×2 array of sub-cells, is used to increase accuracy.

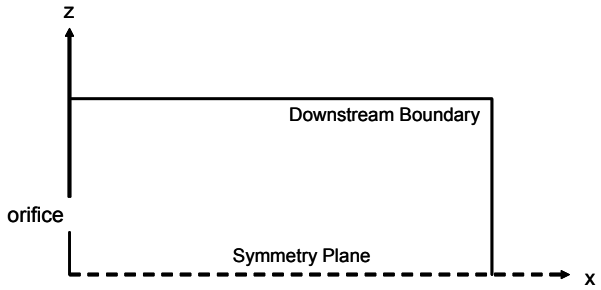

Figure 6. Computation geometry for the interacting jets

The molecular collisions are modeled using the Variable Soft Sphere (VSS) molecular model[12] and the energy exchange between kinetic and internal energies is calculated with the Borgnakke-Larsen model,[12] in which a fixed rotational collision number of $Z_r = 5$ is used. The vibrational relaxation is not considered because the expansion is at room temperature and vibrational degrees of freedom are not active during the expansion process due to the relatively large values of the vibrational relaxation time.[17] The orifice plane (*x=0*) surface is assumed to be a diffusion surface. Our code uses Bird's No-Time-Counter (NTC) scheme.[12] The molecular motion and intermolecular collision are decoupled during a small time interval. To comply with the physics, the time step must be smaller than the average collision interval. The program runs for several steps until it reaches steady state, after which it samples the flow properties at each time step size. To minimize statistical scattering, a large number of simulated molecules and a longer computation beyond the steady state are required. The maximum number of the simulated molecules used in the calculation is approximately 4×10^7. More than 1×10^5 computation steps were

carried out after the steady state has been reached. The length of the time step is set to be $\Delta t = 0.8 t_c$, where t_c is the molecular mean collision time under stagnation conditions.

The stagnation temperature and pressure of the jets are fixed as 227.5K and 870Pa, respectively. The temperature at the orifice plane ($x = 0$ plane) is set to the jet's temperature at the orifice exit. The velocities of the molecules entering through the orifice are generated using Maxwell distribution, with sound speed normal to the upstream boundary. The downstream boundary is assumed to be in vacuum. The DSMC calculations were conducted under various conditions.

V. Results and Discussions

Figs. 7, 8, and 9 show the normalized density, translational temperature, and rotational temperature contours in the *x-z* and *x-y* symmetry planes for $Kn_s = 0.003$ and $L/D = 3$. In this case, the flow field is in the continuum regime. Jet interaction is strong and we can clearly observe an interaction region that is formed near the symmetry plane from the *x-z* plane contours. We can also observe that the interaction region undergoes an expansion in the *y*-direction. Compared to the expansion in the *z*-direction, we can see that the interaction region expands at a faster rate in the y-direction. The reason is that in the planes parallel to the *y-z* plane, the z-momentum is nullified due to the interaction and only the *y*-momentum remains. The translational temperature contour has a similar pattern as the density contour except in the vicinity of the orifice plane. This is due to the fact that the orifice plane is assumed to be hot (has the same temperature with flow in the orifice exit). We can observe that the rotational temperature distribution is significantly different from that of the translational temperature. This is because the rotational temperature in the primary jet rises at a higher off-center angle, while the translational temperature does not behave in the same manner. Figs. 10, 11, and 12 depict the normalized density, translational temperature, and rotational temperature contours for $Kn_s = 0.03$ and $L/D = 3$. In this case, the flow is in the near free molecular regime. Compared to the case for $Kn_s = 0.003$, the interaction region is not clear in the density and rotational temperature contours, but we can still observe a shorter jet interaction region in the translational temperature contour. From the contours on the *x-y* plane, we can see that the rate of expansion in the z-direction has been decreased, compared to the case with $Kn_s = 0.003$

In Fig. 13, the density profiles for $Kn_s \to \infty$ ($L/D = 1.5$, 3, and 6) that are calculated using Eqn. (4) are compared to the DSMC results for the case Kn_s=10. The constants in Eqn. (4) are chosen as:

$$A = 0.56, \qquad k = 3 \quad and \quad \theta_{\max} = 90^{\circ} \tag{26}$$

The comparison shows that in the free molecular regime, the asymptotic model agrees with the DSMC results when $L/D = 3$ and 6. For $L/D = 1.5$, the DSMC results show larger values relative to the results obtained using Eqn. (4). The reason is that when L/D is small, the interaction occurs in the near field of the primary jet, where molecules exhausting from the primary jet have not reached the maximum velocity $u_{\max}$ and thus, the one-jet asymptotic model is not appropriate. Therefore, the relatively slower velocity leads to a larger density, consistent with the continuity equation.

Figs. 14 through 17 give the scaled density profiles along the $(x,0,0)$ axis for $Kn_s = 0.3$, 0.03, 0.003 and 0.0003, respectively. In the scaled plots, ρ/ρ_s is scaled by $(L/D)^2$ and x/D by $(L/D)^{-1}$. When Kn_s is large, we see that the self-similarity phenomenon observed by Zhu still exists. However, even for a very large Kn_s, the density profile for $L/D = 1.5$ is higher than what the scaling law predicts. It can be explained by the failure of the one-jet asymptotic model in the near field. For $L/D = 3$ and $L/D = 6$, the scaling law works better than for $L/D = 1.5$ for the large Kn_s cases. When Kn_s is small, such as $Kn_s = 0.003$ and $Kn_s = 0.0003$, there is a larger difference between the scaled density profiles. This can be explained by the existence of strong interaction shock waves in the interaction region.

Figs. 18 through 20 give the density profiles along the $(x,0,0)$ axis for different values of Kn_s when $L/D = 1.5$, 3.0, and 6.0. These figures show that as Kn_s decreases, the density in the interaction region increases. This agrees with the fact that when Kn_s is small, the interaction effects become more significant and there are more molecules whose z-direction momentum is nullified and that are compressed in the interaction region. Compared

with the differences between the curves in the near free molecular regimes (i.e., between Kn_s = 3, 0.3 and 0.03), the differences between the curves in the near continuum regime (i.e., between Kn_s = 0.03, 0.003, and 0.0003) are very large. This is also due to the existence of the interaction shock waves. As shown in Eqn. (25), the shock greatly decreases the molecular penetration and compresses more molecules in the interaction region.

Figs. 21 through 23 give the *x*-, *y*- and *z*-direction translational temperature profiles for Kn_s = 0.03, 0.003, and 0.0003. It is found that when Kn_s is large, non-equilibrium effects become significant, due to insufficient molecular collisions, which leads to the larger separation in the translational temperatures in different directions. From these plots, we observe that as Kn_s becomes smaller, the *y*-direction translational temperature decreases, while *x*- and *z*-direction translational temperatures increase. The reason is that when the interaction effects become stronger, molecules are more likely to lose y-direction velocity and to increase both the *x*- and *z*-direction velocity.

VI. Conclusion

The interaction effects between parallel jets are analyzed and simulated from the free molecular regime to the continuum regime. The effects of the jet's stagnation Knudsen number Kn_s and the separation distance between the two jets (L/D) is examined using DSMC calculations. The self-similarity of the flow in free molecular regime that was observed by Zhu can be explained by the asymptotic model developed in this paper. This self-similarity is only valid for large values of Kn_s and L/D. For the flow in the continuum or near continuum regimes, the interaction shock waves greatly decrease the molecular penetration. This is analyzed in this paper by introducing a modified Penetration Knudsen Number, Kn_p^*, based on Koppenwallner's definition.

Acknowledgments

The authors would like to thank the Thaerocomp Technical Corporation for providing the financial support for this project.

References

[1]Ashkenas, H. and Sherman, F. S., The Structure and Utilization of Supersonic Free Jets in Low Density Wind Tunnels, Rarefied Gas Dynamics, Fourth Symposium, Vol. II, Academic Press, New York, 1966, pp. 311-330.

[2]Dagum, L. and Zhu S. H. K., DSMC Simulation of the Interaction Between Rarefied Free Jets, July 1993, AIAA paper 93-2872.

[3]Zhu, S. H. K. and Dagum L., A Parametric study of Rarefied Jet Interaction Using DSMC, 6th AIAA/ASME Joint Thermophysics and Heat Transfer Conference, June 1994, Colorado Springs, CO, AIAA-94-2046.

[4]Zhu, S. H. K. and Dagum L., Self-Similarity in Rarefied Jet Interactions - A DSMC Study, 29th AIAA Thermophysics Conference, June 1995, San Diego, CA, AIAA-95-2030.

[5]Koppenwallner, G., Scaling Laws for Rarefied Plume Interaction with Application to Satellite Thrusters, Proceedings of the Fourteenth International Symposium on Space Technology and Science, Tokyo, May 1984.

[6]Dankert, C. and Koppenwallner G., Experimental Study of the Interaction between Two Rarefied Free Jets, Rarefied Gas Dynamics: Proceeding of the 14th International Symposium on Rarefied Gas Dynamics, July 1984, Tsukuba Science City, Japan, pp. 477-484.

[7]Soga, T., Takanishi M. and Yasuhara M., Experimental Study of Interaction of Underexpanded Free Jets, Rarefied Gas Dynamics: Proceedings of the 14th International Symposium on Rarefied Gas Dynamics, July 1984, Tsukuba Science City, Japan, pp. 485-493.

[8]Niim,i T., Fujimoto T. and Taoi N., Flow Fields of Interacting Parallel Supersonic Free Jets, JSME International Journal, Series B, Vol. 39, No. 1, 1996, pp. 95.

[9]Albini, F. A., Approximate Computation of Underexpanded Jet Structure, AIAA Journal, Vol. 3, pp. 1535-1537, 1965.

[10]Hubbard, E. W., Approximate Calculation of Highly Underexpanded Jets, AIAA Journal, Vol. 4, pp. 1877-1879, 1966.

[11]Boyton, F. P., Highly Underexpanded Jet Structure: Exact and Approximate Calculations, AIAA Journal, Vol. 8, pp. 1704, 1967.

[12]Bird, G. A., Molecular Gas Dynamics and the Direct Simulation of Gas Flows. 1st Ed., Oxford Univ. Press, Oxford, 1994.

[13]Schreier, S., Compressible Flow, 1982, Wiley, 1982.

[14]Gldalevich, E., R. L. Boxman and S. Goldsmith, Theory and Modelling of the Interaction of Two Parallel Supersonic Plasma Jets, J. Phys. D: Appl. Phys., Vol. 31, pp. 304-311, 1998.

[15]Hass, B., Flow Resolution and Domain Influence in Rarefied Hypersonic Blunt-Body Flows, AIAA Paper 93-2806, July 1993.
[16]Usami, M. and Teshima K., Molecular Simulation of Rarefied Supersonic Free Jets by DSMC Method, JSME International Journal, Series B, Vol. 42, No. 3, pp 369-376, 1993.
[17]Campargue, R., Lebehot A., and Gaveau M. A.,Internal State Populations in Supersonic Free Jets and Molecular Beams, in Rarefied Gas Dynamics, edited by H.Oguchi, University of Tokyo Press, Tokyo, 1984, pp 551-566.
[18]Ladeinde, F., Cai X. and Li W. A Unified Computational methodology for Rarefied and Continuum Flow Regimes, AIAA-2004-1178
[19]Muntz, E. P., Hamel, B. B. and Maguire, B. L., Some Characteristics of Exhaust Plume Rarefaction, AIAA J., Vol 8, No. 9 (1970), pp. 1651-1658.
[20]Teshima, K. and Usami M. An experimental study and DSMC simulation of rarefied supersonic jets, 20th Rarefied Gas Dynamics, 1996, Ed. by C. Shen, Beijin University Press, 567-572.

a)

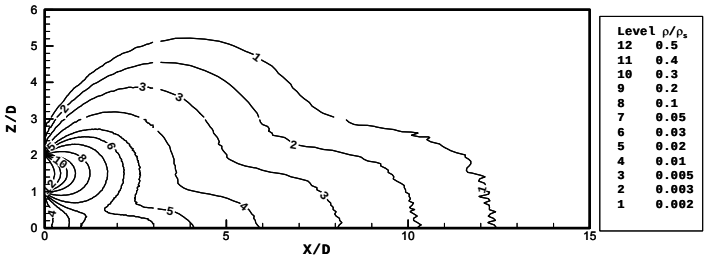

b)

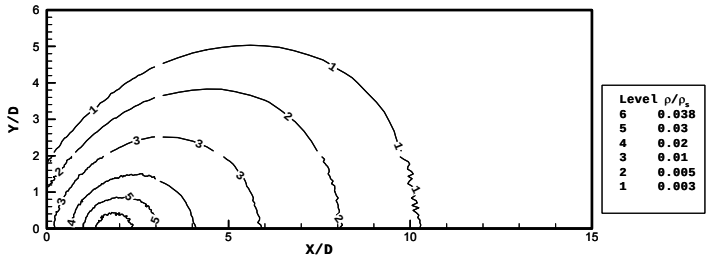

Figure 7. Normalized density contour in a) x-z and b) x-y symmetry planes for Kn_s = 0.003 and L/D = 3

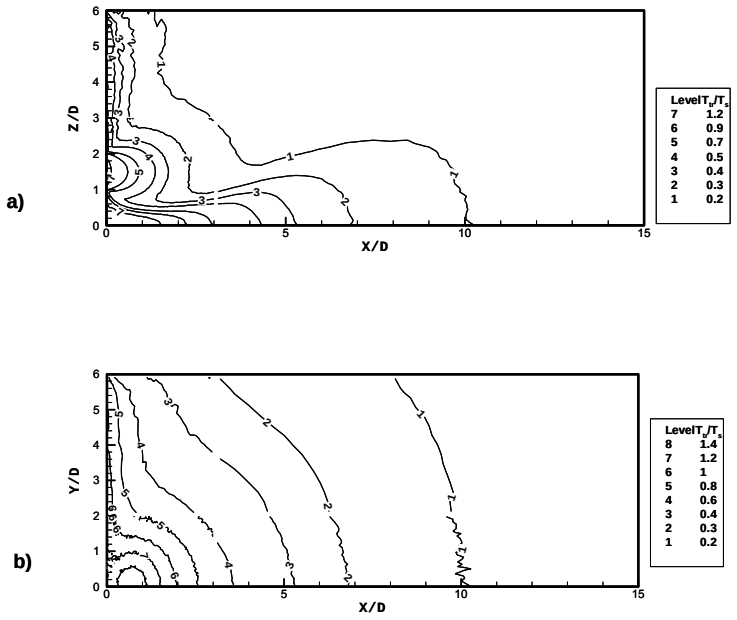

Figure 8. Normalized translational temperature contour in a) x-z and b) x-y symmetry planes for Kn_s = 0.003 and L/D = 3

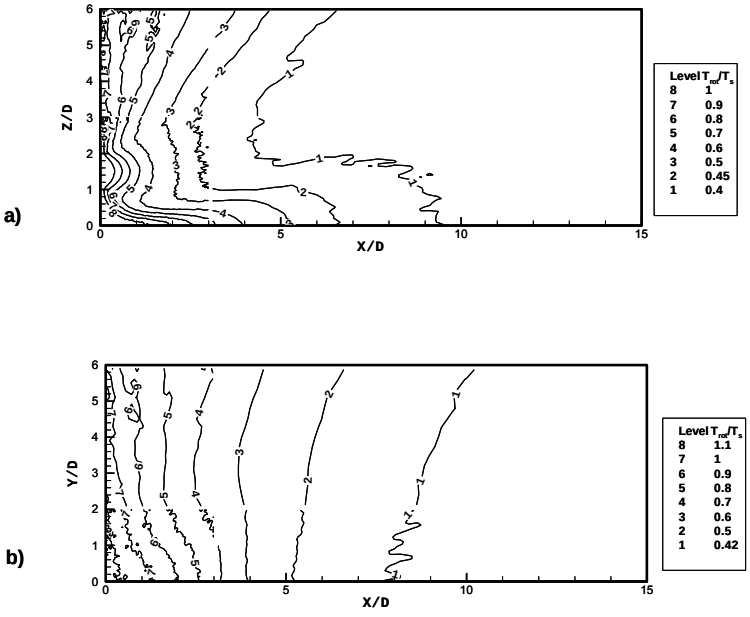

Figure 9. Normalized rotational temperature contour in a) x-z and b) x-y symmetry planes for Kn_s = 0.003 and L/D = 3

a)

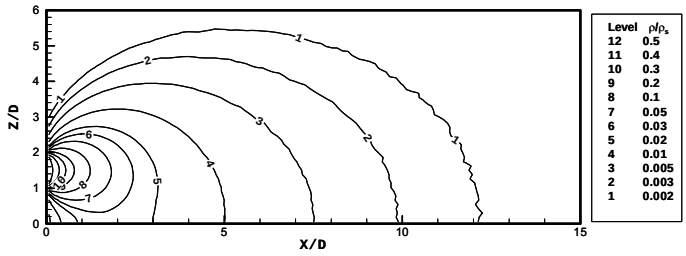

b)

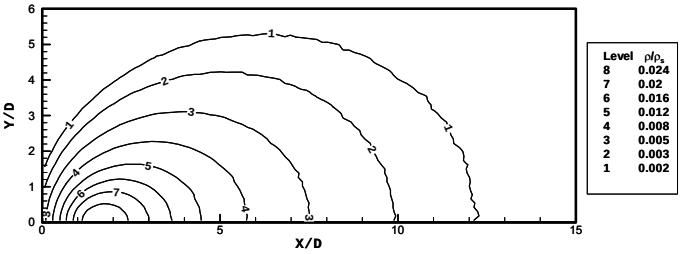

Figure 10. Normalized density contour in a) x-z and b) x-y symmetry planes for Kn_s = 0.03 and L/D = 3

a)

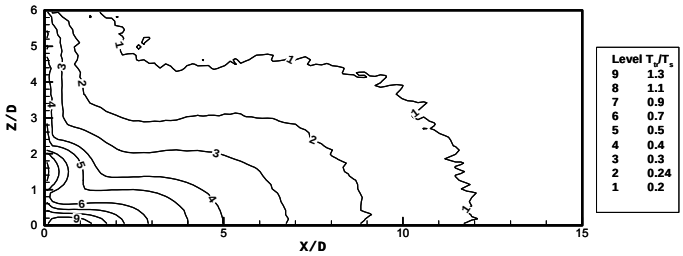

b)

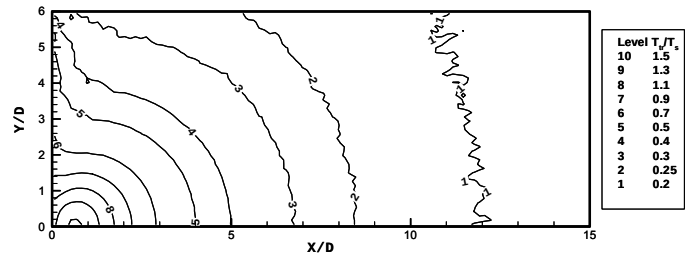

Figure 11. Normalized translational temperature contour in a) x-z and b) x-y symmetry planes for Kn_s = 0.03 and L/D = 3

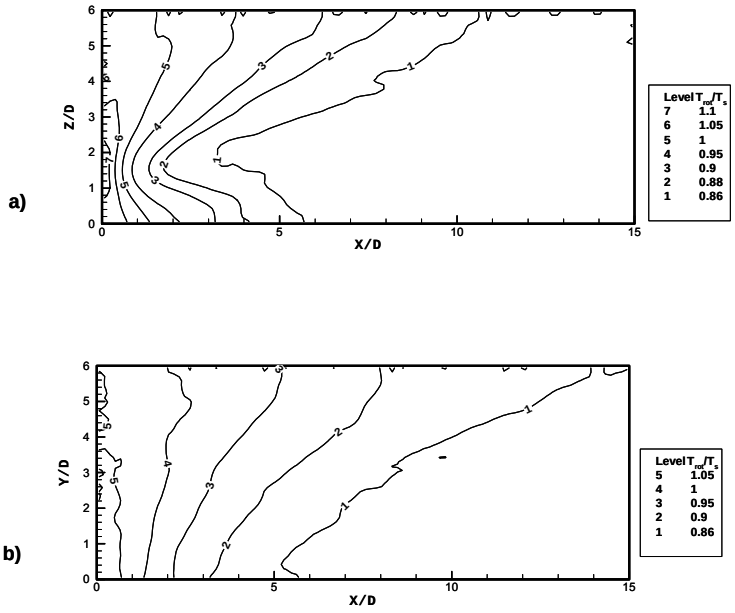

Figure 12. Normalized rotational temperature contour in a) x-z and b) x-y symmetry planes for $Kn_s = 0.03$ and L/D = 3

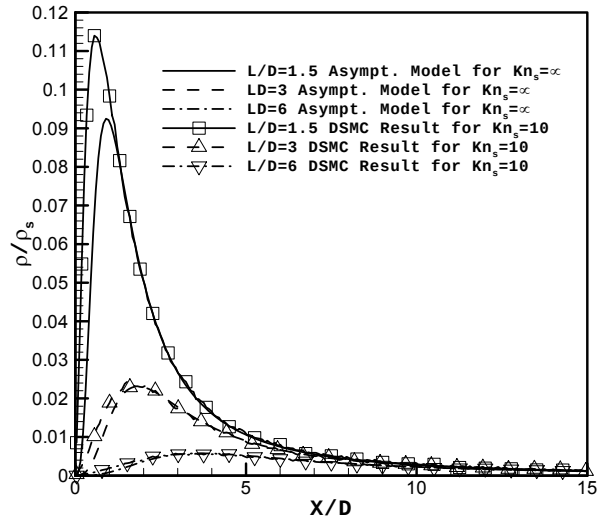

Figure 13. The normalized density profile along the $(x,0,0)$ axis from the asymptotic model ($K\nu_\sigma \to \infty$) and the DSMC ($Kn_s = 10$)

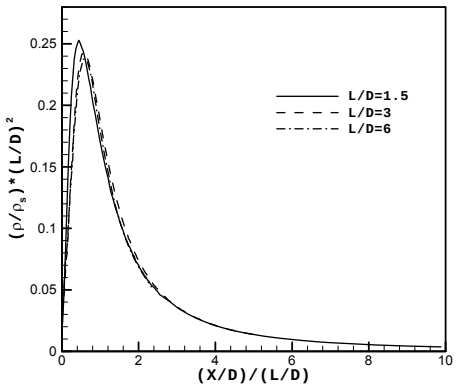

Figure 14. Scaled normalized density profile along the $(x,0,0)$ axis for different values of L/D; Kn_s = 0.3

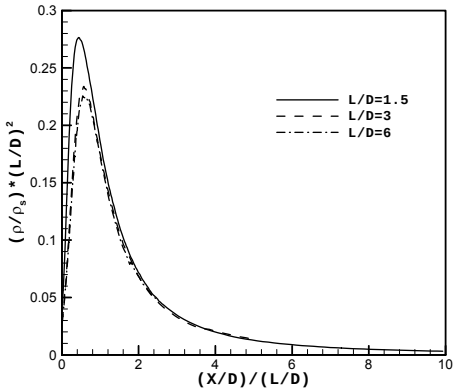

Figure 15. Scaled normalized density profile along the $(x,0,0)$ axis for different values of L/D; Kn_s = 0.03

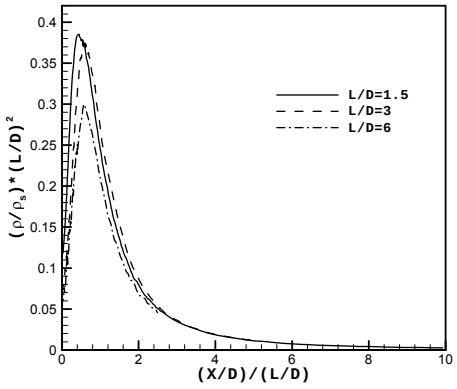

Figure 16. Scaled normalized density profile along the $(x,0,0)$ axis for different values of L/D; Kn_s = 0.003

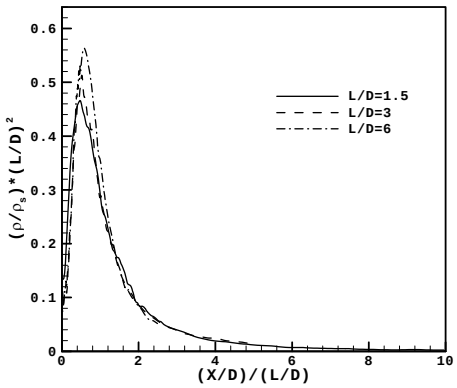

Figure 17. Scaled normalized density profile along the $(x,0,0)$ axis for different values of L/D ; Kn_s = 0.0003

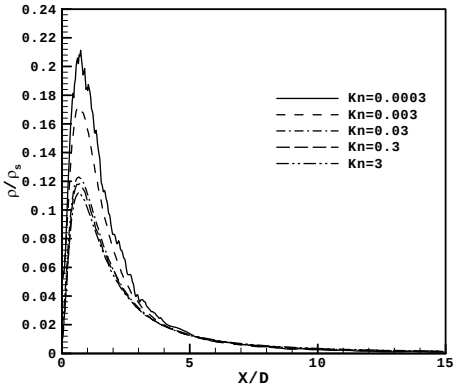

Figure 18. Normalized density profile along the $(x,0,0)$ axis for different Kn_s values when L/D = 1.5

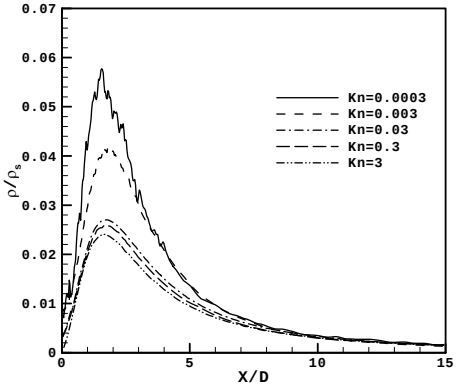

Figure 19. Normalized density profile along the $(x,0,0)$ axis for different Kn_s values when L/D = 3

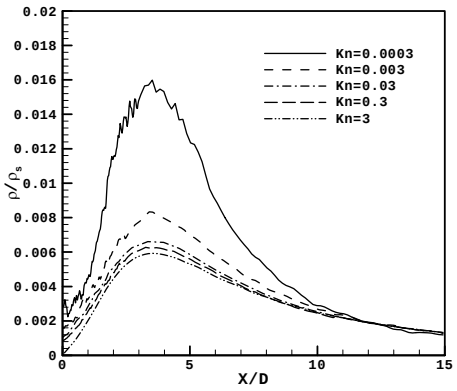

Figure 20. Normalized density profile along the $(x,0,0)$ axis for different Kn_s values when L/D = 6

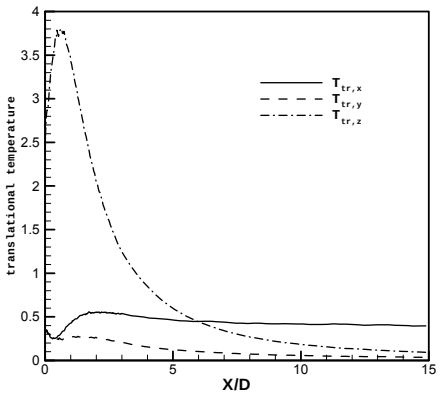

Figure 21. Normalized x-, y- and z-direction translational temperature profile along the $(x,0,0)$ axis for different value of L/D; Kn_s = 0.03

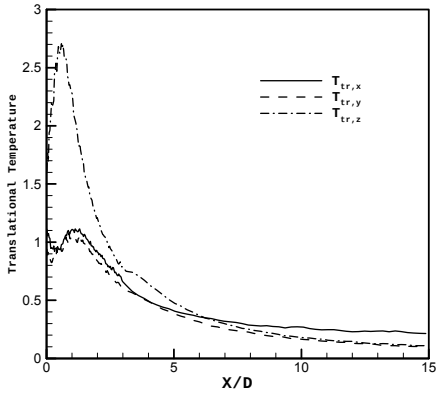

Figure 22. Normalized x-, y- and z-direction translational temperature profile along the $(x,0,0)$ axis for different value of L/D; Kn_s = 0.003

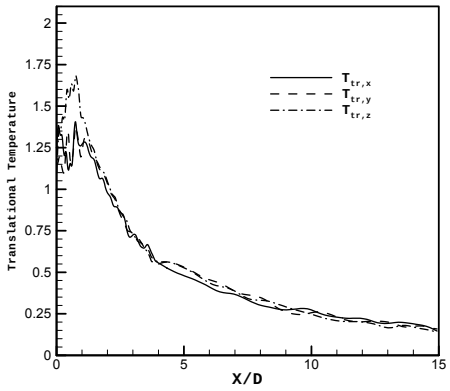

Figure 23. Normalized x-, y- and z-direction translational temperature profile along the $(x,0,0)$ axis for different value of L/D ; Kn_s = 0.0003